# Fe/Thiol Cooperative Hydrogen Atom Transfer Olefin Hydrogenation: Mechanistic Insights that Inform Enantioselective Catalysis

Sarah R. Buzsaki<sup>+1</sup>, Savannah M. Mason<sup>+2</sup>, Padmanabha V. Kattamuri<sup>1</sup>, Juan M. I. Serviano<sup>2</sup>, Dinora N. Rodriguez<sup>1</sup>, Conner V. Wilson<sup>2</sup>, Drew M. Hood<sup>1</sup>, Jonathan D. Ellefsen<sup>2</sup>, Yen-Chu Lu<sup>1</sup>, Jolie Kan<sup>1</sup>, Julian G. West<sup>\*1</sup>, Scott J. Miller<sup>\*2</sup> and Patrick L. Holland<sup>\*2</sup>

**ABSTRACT:** Asymmetric hydrogenation of activated olefins using transition metal catalysis is a powerful tool for synthesis of complex molecules, but traditional metal catalysts have difficulty with enantioselective reduction of electron-neutral, electron-rich, and minimally functionalized olefins. Hydrogenation based on radical, metal-catalyzed hydrogen atom transfer (mHAT) mechanisms offers an outstanding opportunity to overcome these difficulties, enabling mild reduction of these challenging olefins with selectivity that is complementary to traditional hydrogenations with H<sub>2</sub>. Further, mHAT presents an opportunity for asymmetric induction through cooperative hydrogen atom transfer (cHAT) using chiral thiols. Here, we report insights from mechanistic study of an iron-catalyzed achiral cHAT reaction and leverage these insights to deliver stereocontrol from chiral thiols. Kinetic analysis and variation of silane structure point to the transfer of hydride from silane to iron as the likely rate-limiting step. The data indicate that the selectivity-determining step is quenching of the alkyl radical by thiol, which becomes a more potent H-atom donor when coordinated to iron(II). The resulting iron(III)—thiolate complex is in equilibrium with other iron species, including Fe<sup>II</sup>(acac)<sub>2</sub>, which is shown to be the predominant off-cycle species. The enantiodetermining nature of the thiol trapping step enables enantioselective net hydrogenation of olefins through cHAT using a commercially available glucose-derived thiol catalyst, with up to 80:20 enantiomeric ratio. To the best of our knowledge, this is the first demonstration of asymmetric hydrogenation via iron-catalyzed mHAT. These findings advance our understanding of cooperative radical catalysis and act as a proof of principle for development of enantioselective iron-catalyzed mHAT reactions.

#### INTRODUCTION

Historical Background. Asymmetric hydrogenation of olefins is among the most widely used transformations to prepare chiral molecules from prochiral substrates, with classic methods for transition metal-catalyzed asymmetric hydrogenation based on the oxidative addition of H<sub>2</sub> (Scheme 1a).<sup>2</sup> While these reactions are highly efficient and widely used, they historically require substrates with coordinating functional groups for chelating, two-point metal binding to facilitate enantioinduction<sup>3</sup> with limited exceptions.<sup>4</sup> Further, the highest enantioselectivity is observed with electron-poor olefins ("activated olefins"), as interactions between the substrate and the metal are best promoted by substituents on the olefin that are typically electron-withdrawing.5 Recently, hydrogenation of electronneutral, electron-rich ("unactivated"), and minimally functionalized olefins has seen growing improvement and success; however, lower enantioselectivity is commonly observed, and fewer methods are available.6

In this context, radical hydrofunctionalization enabled by metal-catalyzed hydrogen atom transfer (mHAT) reactions have particular promise as they do not require metal coordination of the olefin for reactivity. Mechanistically, mHAT involves a metal-hydride intermediate that transfers H• to the olefin to generate an alkyl radical that may be trapped under mild conditions. mHAT chemistry has been used for olefin hydrofunctionalizations with inexpensive Fe, Co, and Mn catalysts and exhibits excellent functional group tolerance, permitting late-stage functionalizations in total synthesis. 9

In 2014, the Shenvi and Herzon groups independently published olefin hydrogenation by manganese- and cobalt-catalyzed mHAT respectively, trapping the transient alkyl radical with a second HAT step. <sup>8b, e, f, n</sup> mHAT has some advantages over typical transition metal-catalyzed hydrogenations of olefins, which proceed by additions of H<sub>2</sub>. First, unactivated olefins react well in mHAT methods, enabled by the high reactivity (low bond dissociation energy) of the weak metal-hydride bond. <sup>8b</sup> The hydride source and reductant in mHAT is a silane or borohydride, <sup>8a, 8b, 8n, 10</sup> enabling selective monoreduction of a polyalkene via stoichiometry control, which would be more challenging using a traditional hydrogenation in which the reductant is 1 atm of H<sub>2</sub> or solvent alcohol. Finally, the radical mechanism offers complementary selectivity relative to a typical transition-metal catalyzed mechanism, with improved chemoselectivity and preservation of sensitive functional groups. <sup>8a, 8b, 8n, 10</sup>

One problem with these single-catalyst mHAT systems (Scheme 1b) is that they require at least stoichiometric loading of an oxidant, such as tert-butyl hydroperoxide (TBHP), which is necessary to turn over the  $M^{2+}/M^{3+}$  cycle. While enabling, the inclusion of this oxidant reduces the atom economy of the reaction and can introduce some additional safety considerations. <sup>11</sup> In 2020, West and coworkers addressed this problem with the cooperative hydrogen atom transfer

<sup>&</sup>lt;sup>1</sup>Department of Chemistry, Rice University, Houston, Texas 77030, United States

<sup>&</sup>lt;sup>2</sup>Department of Chemistry, Yale University, New Haven, Connecticut 06520, United States

Scheme 2. Previously proposed mechanism for olefin hydrogenation via iron and thiol cHAT

Adapted with permission from Reference 12. Copyright 2020 American Chemical Society.

112, 113 - aikyi or 11

(cHAT) method for the chemoselective hydrogenation of unactivated olefins (Scheme 1c). <sup>12</sup> In cHAT, an Fe-based catalyst is complemented by a catalytic amount of a thiol that rapidly traps the alkyl radical to give the net hydrogenation product. The catalysts can be regenerated while avoiding the use of a stoichiometric oxidant. The cHAT system provides a facile method for olefin hydrogenation with up to 93% yield.

The original report of olefin hydrogenation by cHAT suggested a mechanism with two intersecting cycles (Scheme 2).<sup>12</sup> In the iron cycle (left/red intermediates), the iron(III) catalyst reacts with PhSiH<sub>3</sub> to generate the iron(III) hydride complex, which undergoes mHAT to the unactivated olefin I to generate the alkyl radical II. Then, a thiol HAT cycle (right/blue intermediates) provides the radical trap to generate hydrogenated product III. The thiyl radical then intercepts the iron(II) intermediate to regenerate the iron(III) and thiol. One striking feature of the system is the overall compatibility of intersecting cycles predicated on the mutual roles for Febased catalyst and thiols. A number of experiments supported this mechanistic model: TEMPO inhibition suggests the presence of radical intermediates; deuterium labeling studies support that the EtOH/thiol exchange is the source of the second H., which is delivered to the alkyl radical through the thiol catalytic cycle. However, important mechanistic questions remained, particularly about the intersection of the two cycles. For example, how does the system avoid the plausible inhibition of the iron catalyst by thiol/thiolate donors? What is the speciation of the iron catalyst? Is the radical trap the free thiol or an Fe-thiol complex? Additionally, can chiral information be introduced via the thiol to influence the stereochemistry of the second C-H bond forming event? These questions were the motivating force behind the study described herein.

Asymmetric Hydrogen Atom Transfer Reactions. Several recent advances have been made in the development of methods for enantioselective mHAT olefin hydrofunctionalization, each of which uses cobalt catalysts with chiral ligands. These examples include both intramolecular and intermolecular reactions with alcohols, heteroarenes, and various nitrogen sources. To the best of our knowledge, however, no studies have reported any enantioselective mHAT olefin functionalization or hydrogenation that uses an

Fe-based catalyst. This difference between metals may be due to the higher bond dissociation free energy (BDFE) of the Co–C bond in the cobalt(IV)–alkyl intermediate (calcd. 22 kcal/mol $^{16}$ ) relative to the very weak BDFE for the putative Fe–C bond in the iron(III)–alkyl intermediate (calcd. 1.5 kcal/mol $^{17}$ ). Indeed, organocobalt species arising from cobalt mHAT can be isolated,  $^{16,18}$  while analogous alkyl intermediates from iron mHAT have yet to be characterized experimentally. The relative stability of  $\left[\text{Co}^{\text{IV}}\right]$ –alkyl intermediates in particular enables them to undergo nucleophilic attack via an S $_{\text{N}}2$  mechanism and to provide enantioinduction through use of a chiral ligand.  $^{8b,\,15b,\,16,\,18\cdot19}$  In contrast, the Fe–C bond is too weak to proceed through a similar S $_{\text{N}}2$  mechanism, homolyzing before any opportunity arises for chiral information to be transmitted by a supporting ligand.

The presence of the thiol/thiyl catalytic cycle in cHAT olefin hydrogenation provides a unique opportunity to circumvent this challenge through use of a chiral thiol co-catalyst, introducing stereochemistry during the alkyl radical trapping/C–H bond-forming step. We note that thiols have been used as chiral HAT catalysts to provide stereocontrol through asymmetric delivery of H• to alkyl radicals. In early studies, Roberts pioneered the use of chiral thioglycosides as HAT catalysts to provide enantioinduction in olefin hydrosilylation. Recently, the Ye group developed methods with both chiral thioglycosides and cysteine-based peptide catalysts for asymmetric olefin functionalization. In additional applications of cysteine-based peptide catalysts as chiral HAT catalysts, the Miller and Knowles groups reported enantioselective HAT in the deracemization of cyclic ureas<sup>22</sup> and the hydroamination of olefins. In the deracemization of cyclic ureas<sup>23</sup>

From these examples and our working understanding of cHAT, we hypothesized that a chiral thiol catalyst could be used to confer asymmetry in Fe and thiol cHAT olefin hydrogenation. Here, we demonstrate the plausibility of these ideas, starting with kinetic analysis, spectroscopy, and computations that enable better understanding of the symbiotic operation of the two cycles in Scheme 2. Using this mechanistic insight, we then show that chiral thiol catalysts can indeed lead to significant stereocontrol in olefin hydrogenation. With selectivities of up to 80:20 er, though modest, this work provides the first demonstrations of asymmetric induction in iron-catalyzed mHAT reactions. These results show the promise for further development of enantioselective catalysts with mHAT and provide firm mechanistic footing for such studies.

#### RESULTS AND DISCUSSION

Initial Kinetic Analysis Using PhSiH<sub>3</sub>. The reaction orders in the observed rate law for the achiral cHAT olefin hydrogenation reaction (Figure 1) were evaluated by monitoring product formation using GC. We used two complementary methods to increase our confidence about the conclusions. The first was to assess the entire reaction course graphically with variable time normalization analysis (VTNA).<sup>24</sup> The second was to use initial rate measurements. Employing each kinetic technique, the order of the rate dependence on PhSiH<sub>3</sub> can be reasonably fit to either +0.5 or +1 order in [PhSiH<sub>3</sub>], with a clear positive rate dependence (Figure 1 for VTNA, see SI for initial rate data). The rate dependences on [olefin] and [thiol] were found to be zero order (see SI for detailed analysis).

Surprisingly, the best fits for the rate (using VTNA or initial rates) indicated a pseudo-zero order dependence on [Fe]. Using VTNA, there is a deviation at later time points, prompting us to test for catalyst deactivation using a method derived from reaction progress kinetic analysis.<sup>25</sup> Two hydrogenation reactions were conducted in parallel, with the first unchanged from standard conditions. The second reaction started with lower concentration of starting material but included the independently prepared product to mimic a partially complete reaction, but without any catalyst deactivation.

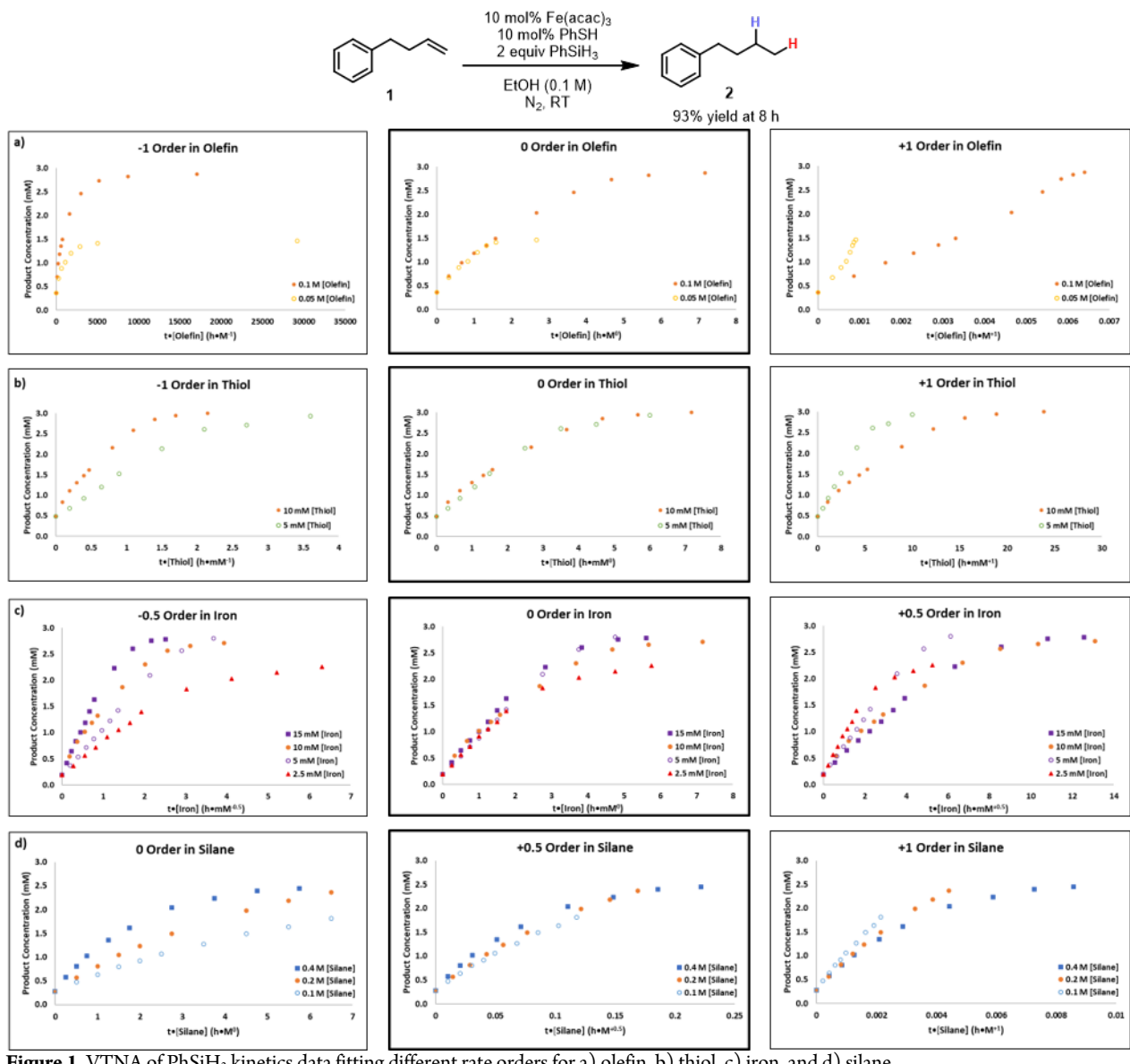
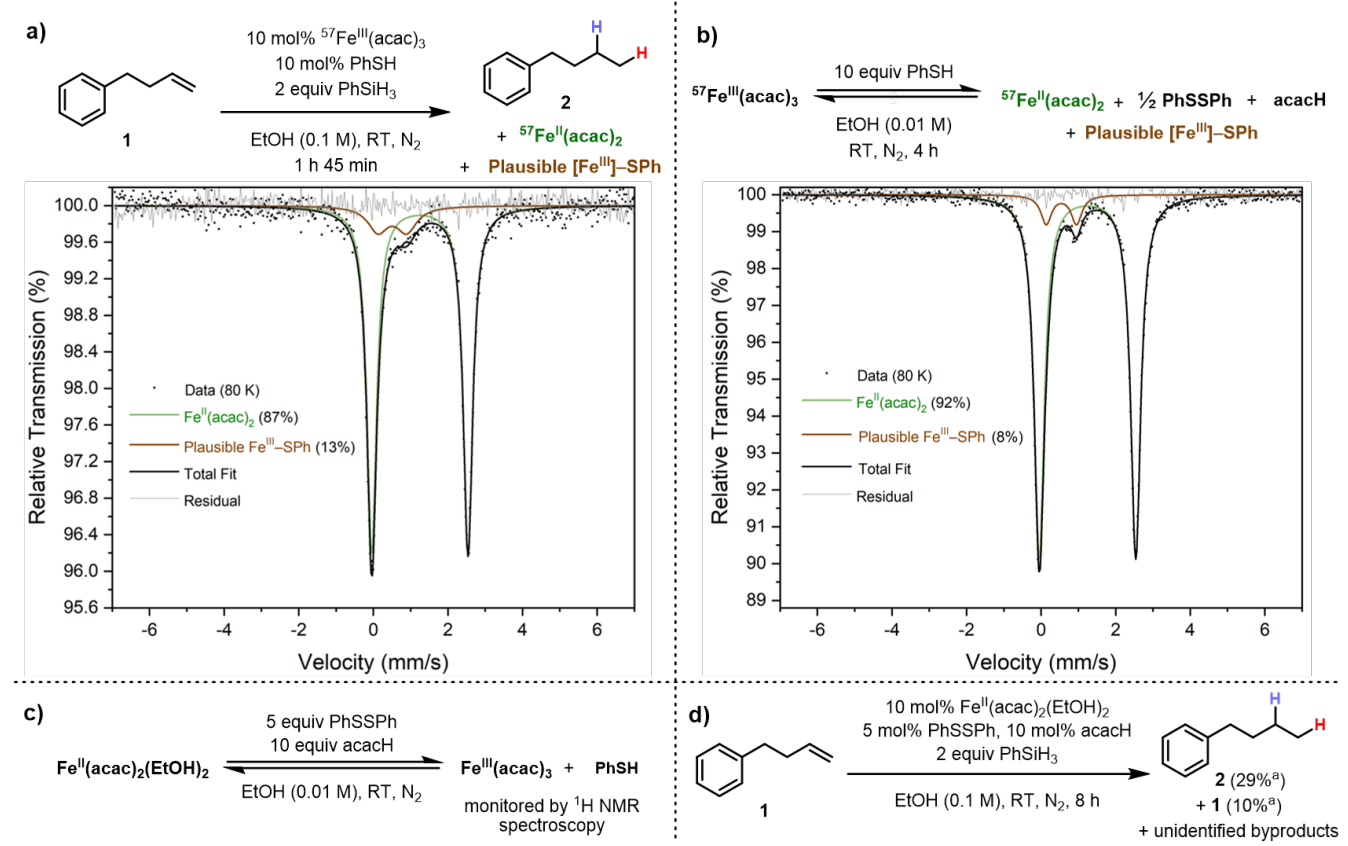


Figure 1. VTNA of PhSiH<sub>3</sub> kinetics data fitting different rate orders for a) olefin, b) thiol, c) iron, and d) silane.



**Figure 2.** a) Olefin hydrogenation reaction monitored by freeze-trapped solution-state Mössbauer spectroscopy. The spectrum has been fit to the following parameters for Fe<sup>II</sup>(acac)<sub>2</sub> —  $\delta$  = 1.25 mm/s,  $|\Delta E_Q|$  = 2.58 mm/s,  $\Gamma$  = 0.31 mm/s and for the plausible [Fe<sup>III</sup>]–SPh complex —  $\delta$  = 0.51 mm/s,  $|\Delta E_Q|$  = 0.77 mm/s,  $\Gamma$  = 0.65 mm/s. b) Reduction of iron(III) to iron(II) by PhSH, monitored by freeze-trapped solution-state Mössbauer spectroscopy. The spectrum has been fit to the following parameters for Fe<sup>II</sup>(acac)<sub>2</sub> —  $\delta$  = 1.24 mm/s,  $|\Delta E_Q|$  = 2.58 mm/s,  $\Gamma$  = 0.33 mm/s and for the plausible [Fe<sup>III</sup>]–SPh complex —  $\delta$  = 0.54 mm/s,  $|\Delta E_Q|$  = 0.81 mm/s,  $\Gamma$  = 0.34 mm/s. c) Oxidation of iron(II) to iron(III). d) Olefin hydrogenation reaction with iron(II) and PhSSPh. <sup>a</sup>Percent yield determined by <sup>1</sup>H NMR with 1,4-bis(trimethylsilyl)benzene as internal standard.

Importantly, the two reaction profiles *do not overlay* (see SI), suggesting that catalyst deactivation occurs during catalysis. This result could help explain the pseudo-zero rate order in catalyst and is addressed in more detail below ("Identifying the Catalyst Deactivation Pathway"). Perhaps the most salient conclusion from the kinetics, however, is that while the rate is independent of olefin and thiol concentrations, it is dependent on [silane], suggesting that silane is part of the turnover-limiting step. This finding is consistent with mechanistic studies on iron-catalyzed mHAT olefin-olefin cross-coupling, which shares several common intermediates. Sh, 17 The slowest step in the coupling reaction is formation of the [Fe<sup>III</sup>]—H intermediate, which is high-energy and requires overcoming a high-energy transition state for its formation. This seems to be the case for the cHAT hydrogenation studied here as well.

**Kinetics Using PhSi(OiPr)H2.** To further investigate the role of silane in determining the rate, we tested  $PhSi(OiPr)H_2$ , which was previously reported by Shenvi and coworkers to be highly active in mHAT reactions. We found that replacing  $PhSiH_3$  with  $PhSi(OiPr)H_2$  significantly increases the rate of cHAT olefin hydrogenation, achieving the same >90% yield in 15 minutes rather than 8 hours. This finding supports the hypothesis that silane is involved in the turnover-limiting step of the catalytic reaction.

Since the reaction is performed in ethanol, we also assessed whether solvolysis of PhSi(O*i*Pr)H<sub>2</sub> to PhSi(OEt)H<sub>2</sub> occurs under the reaction conditions. First, we monitored a solution of 0.2 M

PhSi(OiPr)H<sub>2</sub> in EtOH by GC, which showed that formation of PhSi(OEt)H<sub>2</sub> was already 91% complete within 2 min and is fully complete within 17 min. We also found that the catalytic hydrogenation was more rapid in ethanol than isopropanol (see details in SI). This indicates that the solvolysis of the silane is rapid under catalytic conditions, which is consistent with a lack of significant induction period. Efforts to establish the rate law with the alkoxysilanes were unsuccessful (see SI), perhaps due to confounding kinetic contributions from solvolysis. We tentatively attribute the non-integer rate order for silane to silane decomposition via the known iron(II)-catalyzed solvolysis to form inactive silyl products, such as PhSi(OEt)<sub>2</sub>H and PhSi(OEt)<sub>3</sub>. 8h, 17

To our knowledge, others have not considered this explanation for solvent dependence of mHAT rates. Sth, 26 This implies that, in the future, other mHAT reactions could also be facilitated by using smaller alcohols as solvents because of decreased steric hindrance in transferring hydride from silane to the transition metal during the turnover-limiting step. Of course, the generality of this effect will need to be assessed in each reaction system separately.

Testing an Alternative Explanation – Silane Pre-Activation. We also considered that rate-limiting silane pre-activation through reaction with EtOH could explain the presence of only silane and not iron in the rate law of the PhSiH<sub>3</sub> system. Specifically, formation of the more active alkoxysilane species, PhSi(OEt)H<sub>2</sub>, from PhSiH<sub>3</sub> could be catalyzed by ethoxide from solvent autoionization or by

EtOH directly. However, we were able to rule out this hypothesis by monitoring a solution of PhSiH<sub>3</sub> in EtOD by <sup>1</sup>H NMR spectroscopy over 10 h, during which we observed no detectable formation of new compounds. Therefore, uncatalyzed reaction of silane with solvent is an unlikely rate determining step.

Identifying the Catalyst Deactivation Pathway. In order to assess the nature of catalyst deactivation as identified in the kinetics, we examined the iron speciation during the catalytic reaction via <sup>57</sup>Fe Mössbauer spectroscopy. Solutions flash-frozen during catalysis (at approximately 45% conversion) using <sup>57</sup>Fe<sup>III</sup>(acac)<sub>3</sub> showed that the majority of iron in the reaction was present as Fe<sup>II</sup>(acac)<sub>2</sub> (Figure 2a). We considered that iron reduction could arise from homolysis of iron(III)-hydride and/or iron(III)-alkyl bonds, 8b, 8h, 17 or from reduction by thiol. Examples from the literature abound for reduction of iron(III) by thiols, <sup>27</sup> and we sought to understand whether thiol plays a role in the formation of Fe<sup>II</sup>(acac)<sub>2</sub> in cHAT olefin hydrogenation. Therefore, we treated Fe<sup>III</sup>(acac)<sub>3</sub> with 10 equiv PhSH, which resulted in rapid, complete consumption of Fe<sup>III</sup>(acac)<sub>3</sub> with formation of Fe<sup>II</sup>(acac)<sub>2</sub> and PhSSPh, as identified by Mössbauer and <sup>1</sup>H NMR spectroscopies (Figure 2b). This deactivation path is further supported by the observed suppression of hydrogenation reactivity when running the reaction with excess thiol (see SI). Thus, the added thiol is a feasible culprit that leads to the inactive  $\mathsf{Fe}^{\scriptscriptstyle{\mathrm{II}}}(\mathsf{acac})_2$  observed in the hydrogenation reaction. With only 1 equiv PhSH to 1 equiv Fe<sup>III</sup>(acac)<sub>3</sub>, however, only partial deactivation of Fe<sup>III</sup>(acac)<sub>3</sub> to Fe<sup>II</sup>(acac)<sub>2</sub> was observed by <sup>1</sup>H NMR spectroscopy (see SI). This is a plausible explanation for why the reaction is not completely suppressed under catalytic conditions.

Interestingly, this reduction of iron(III) by thiol is reversible. We found that the reaction of Fe<sup>II</sup>(acac)<sub>2</sub>(EtOH)<sub>2</sub>, PhSSPh, and acetylacetone (acacH) produced Fe<sup>III</sup>(acac)<sub>3</sub> as observed by <sup>1</sup>H NMR spectroscopy (Figure 2c). However, the efficiency of the iron oxidation pathway is impacted by the low solubility of Fe<sup>II</sup>(acac)<sub>2</sub> in EtOH. To further probe the iron oxidation pathway, we tested the olefin hydrogenation reaction using 10 mol% Fe<sup>II</sup>(acac)<sub>2</sub>(EtOH)<sub>2</sub>, S mol% PhSSPh, and 10 mol% acacH (Figure 2d). After 8 h, we observed 29% yield of hydrogenated product with incomplete consumption of olefin starting material. The observation of very sluggish catalysis indicates that the catalyst may be rescued, but this is not kinetically competent on the timescale of the catalytic reaction. Thus, we propose that the reason for the apparent zero-order rate dependence on [Fe] is that most of the iron in the reaction becomes

Scheme 3. a) Olefin hydrogenation reaction with iron(II) and PhSSPh in the absence of acacH; b) Proposed pathway for [Fe<sup>III</sup>]-SPh in equilibrium with on-cycle species, [Fe<sup>III</sup>]-OEt

[Fe] = Fe(acac)<sub>2</sub>

"Percent yield determined by <sup>1</sup>H NMR with 1,4-bis(trimethylsilyl)benzene as internal standard.

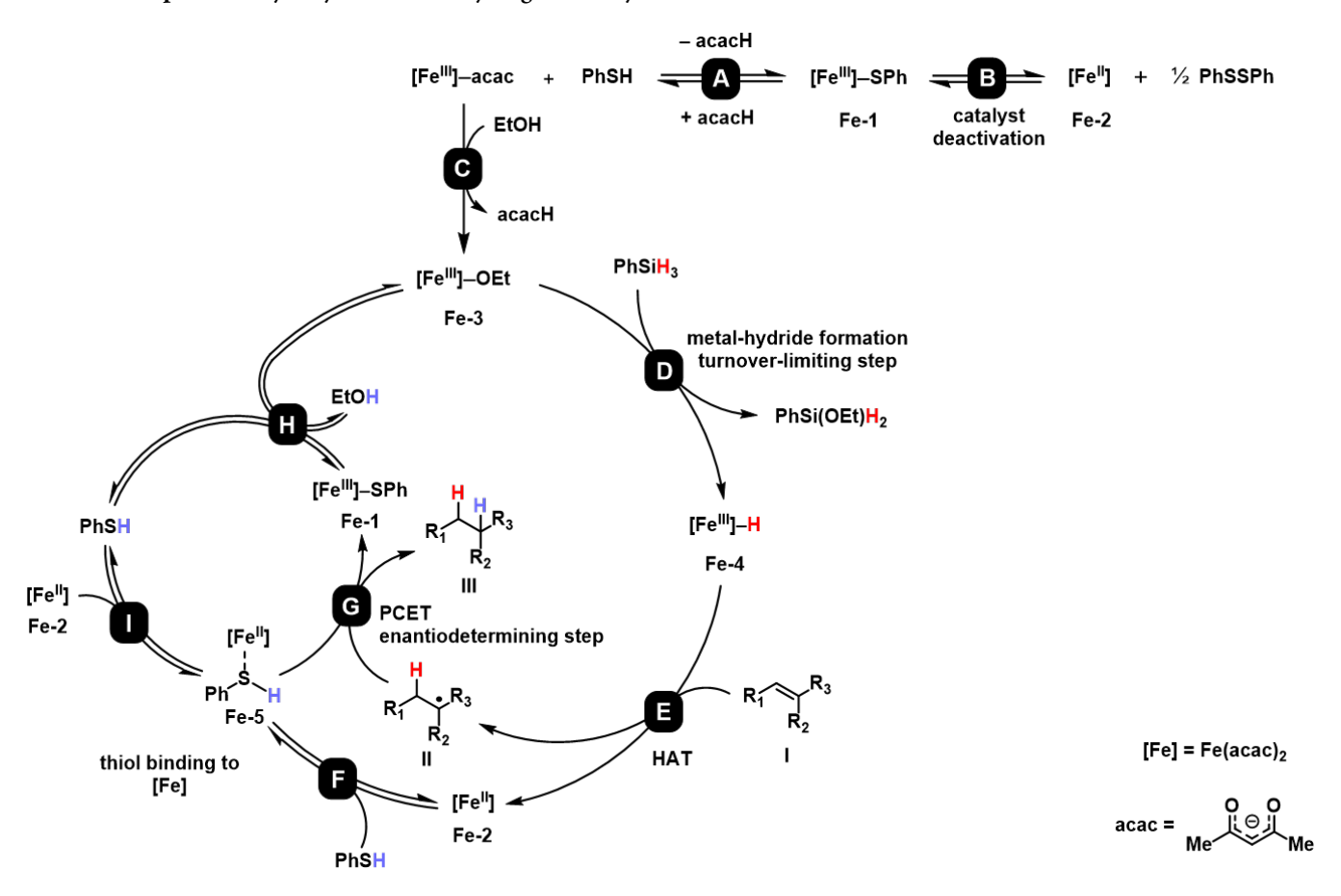
reduced and inactive. A small amount of catalyst (independent of the amount of *added* iron, since it is limited by the solubility of  $Fe^{II}(acac)_2$ ) is participating in the catalytic reaction.

Plausible [Fe<sup>III</sup>]-Thiolate Complex. During these efforts to identify catalyst deactivation, we also observed an unknown iron(III) species, which accounted for ~10% of the iron in the Mössbauer spectra of both the olefin hydrogenation and the iron reduction reaction (Figures 2a and 2b). As the parameters for this species were not consistent with those previously reported for an iron(III)ethoxide complex ([Fe<sup>III</sup>(acac)<sub>2</sub>( $\mu$ -OEt)]<sub>2</sub>,  $\delta$  = 0.54 mm/s,  $|\Delta E_{Q}|$  = 0.51 mm/s), 17 we hypothesized that this unknown iron species could be an iron(III)-thiolate complex. As noted at the outset, the plausible interaction of the Fe-based catalysts with the thiol/thiyl catalyst represents one of the most intriguing aspects of thiol cHAT. Attempts to isolate and crystallize the iron(III) complex were unsuccessful. Therefore, we turned to density-functional theory (DFT) calculations to compute Mössbauer parameters for plausible iron(III)-thiolate complexes, for comparison to Mössbauer spectra of the mixtures generated in situ. We found that the calculated Mössbauer parameters for several possible iron(III)—thiolate complexes, including monomers and bridging diiron complexes, are consistent with the experimental values of the unknown complex (see SI). The broadness of the peak observed in Figure 2a suggests that it is not a single thiolate species; it may be a mixture of complexes with differing nuclearities. Though the precise structure is not clear from these spectroscopic measurements, these studies support the feasibility of iron-thiolate species.

The iron(III)–thiolate complex may be an intermediate of the iron reduction and/or an intermediate of the catalytic cycle. To probe the latter proposal, we tested the hydrogenation reaction with 10 mol%  $Fe^{II}(acac)_2(EtOH)_2$  and 5 mol% PhSSPh in the absence of acacH (Scheme 3a). After 8 h, we observed 8% product formation and incomplete consumption of starting material. In the absence of acacH, the formation of product may proceed through the  $[Fe^{III}]$ –SPh intermediate (Scheme 3b). Our results are consistent with  $[Fe^{III}]$ –SPh being on-cycle or in equilibrium with an on-cycle species.

**Thiol Binding to Iron(II).** In the iron-catalyzed olefin-olefin cross-coupling via HAT, we proposed that the alkyl radical generated following HAT is quenched via proton-coupled electron transfer (PCET) from an iron(II) ethanol complex, a step which is enabled by the lowering of the O–H BDFE upon coordination of EtOH to the iron center. The cHAT olefin hydrogenation system presents an opportunity to form an analogous iron(II) thiol complex, which would likewise have a decreased S–H BDFE. The feasibility of an iron(II)—thiol interaction is supported by literature suggesting

Scheme 4. Proposed catalytic cycle for olefin hydrogenation by iron and thiol cHAT<sup>a</sup>



<sup>a</sup>Proposed neutral ligands, such as EtOH, have been omitted for clarity. Step F and Step I are identical but are shown twice for clarity.

that cysteine binds as a neutral donor to iron(II) heme complexes. While Lewis basic ligands with oxygen, nitrogen, and phosphorus donor atoms are known to coordinate to  $Fe^{II}(acac)_2$ , to the best of our knowledge no studies have yet reported evidence for binding of neutral sulfur-based ligands. Therefore, we sought to experimentally probe whether thiol binds to iron(II) under conditions relevant to olefin hydrogenation.

We began by monitoring a mixture of  $Fe^{II}(acac)_2(EtOH)_2$  and 10 equiv PhSH in ethanol- $d_6$  by  ${}^{1}H$  NMR spectroscopy. We observed no evidence of thiol binding, potentially due to competition with EtOH. Accordingly, we monitored the reaction in 95:5 toluene- $d_8$ : ethanol- $d_6$ . At low temperatures, we observed peak broadening and a shoulder peak by  ${}^{1}H$  NMR spectroscopy, indicating a change in speciation of  $Fe^{II}(acac)_2(EtOH)_2$ . Though the broad peaks do not enable us to elucidate the structure, this observation is consistent with weak PhSH binding to iron(II), which leads to an equilibrium mixture containing some amount of thiol complex.

Using DFT calculations (B3LYP/ZORA-def2-TZVP), we calculated the binding energy of the thiol in the hypothetical molecule  $Fe^{II}(acac)_2(EtOH)(PhSH)$  to be 19 kcal/mol. To further investigate the effects of thiol coordination to iron(II), we calculated the BDFE of the S–H bond in this iron(II) complex. Upon binding to  $Fe^{II}(acac)_2(EtOH)$ , the BDFE of the S–H bond in PhSH is predicted to weaken from 82 to 66 kcal/mol (see SI for additional BDFE calculations). Therefore, binding to iron(II) would make the S–H bond weaker than the O–H bond iniron(II) ethanol complexes (calcd. 70 kcal/mol), and it could react rapidly with the alkyl radical.

Indeed, attempts to locate a transition state along the pathway of hydrogen atom transfer showed that the reaction is practically barrierless. Thus, all of our evidence suggests that an iron(II)-thiol complex can quench the alkyl radical extremely rapidly.

**Proposed Catalytic Cycle.** Based on the above experiments and analysis, a catalytic cycle for olefin hydrogenation by iron and thiol cHAT is proposed in Scheme 4. In a catalyst deactivation pathway,  $Fe^{III}(acac)_3$  reacts with PhSH to form  $Fe^{II}(acac)_2$  (**Fe-2**) and PhSSPh, proceeding through the iron(III)–thiolate intermediate **Fe-1** (Steps **A** and **B**). This process is reversible; however, the poor solubility of  $Fe^{II}(acac)_2$  limits the rate of oxidation of iron to re-enter the cycle.

We propose that the low concentration of Fe<sup>III</sup>(acac)<sub>3</sub> forms the active iron(III)-ethoxide catalyst **Fe-3** (Step **C**), which reacts with PhSiH<sub>3</sub> in the turnover-limiting step to form iron-hydride **Fe-4** (Step **D**). Following HAT to the olefin **I**, an alkyl radical **II** is generated (Step **E**). PhSH then coordinates to the resulting iron(II) intermediate **Fe-2** to form an iron(II) thiol complex **Fe-5** (Step **F**). While we cannot rule out that alkyl radical **II** is quenched by free thiol, we propose that **II** is primarily quenched via PCET from **Fe-5**, due to the lowered S-H BDFE upon binding to iron. This generates the hydrogenated product **III** and the iron(III)-thiolate complex **Fe-1** (Step **G**). Finally, **Fe-1** undergoes ligand exchange to regenerate PhSH and **Fe-3**. This mechanism is supported by observation of Fe<sup>II</sup>(acac)<sub>2</sub> and a likely iron(III)-thiolate species by Mössbauer spectroscopy, as well as the stoichiometric reactions shown in Figure 2.

Evaluating the Potential for Enantioinduction. In the catalytic cycle shown in Scheme 4, a stereogenic center is set when radical II reacts with a formal H-atom donor. Accordingly, we envisioned that use of a chiral thiol may allow Step G to serve as an enantiodetermining step. To assess the possibility of enantioselective catalysis, we designed a small set of prochiral substrates. We took inspiration from multiple sources, opting for a heterocyclic substrate with exocyclic olefin modeled after the lactone substrates utilized by Roberts and coworkers. <sup>20a, 30</sup> The exocyclic olefins that lead to the products shown in Scheme 5 also would proceed through intermediate radicals that would bear structural homology to the alkyl radical intermediate accessed in recent work of Miller, Knowles, and coworkers, in which enantioselective HAT from a thiol was integral to substrate deracemization.<sup>22</sup> With synthetic accessibility in mind, we thus prepared the N-aryl cyclic ureas and N-aryl thiazolidines 3a-d. Of note, thiazolidines are biologically-active structural scaffolds with various documented applications.31

Intriguingly, we found minimal to low conversion with the cyclic ureas **3a-b**, potentially arising from inhibition through coordination with the iron catalyst. However, the thiazolidines were well tolerated, affording higher conversion to product. In particular, the methylated thiazolidine **3d** reached 92% conversion to product **4d** within 48 hours and was therefore prioritized for further study.

We performed preliminary optimization of the achiral method with the model substrate 3d, beginning with assessment of the metal catalyst. We screened several commercially available metal catalysts with established reactivity in mHAT transformations (Table 1, entries 1-3). Se, SE, SE, SE Ultimately, we found that other catalysts did not perform better than Fe(acac)<sub>3</sub>, in agreement with the original report of the cHAT system (Table 1, entry 1). We found that a slightly higher loading of 15 mol% metal catalyst (Table 1 entry 4) afforded higher conversion to product. Higher concentration (Table 1 entry 5) had minimal impact on conversion, so we moved forward with conditions as in entry 4. Additional screening results are detailed in the SI.

With the development of a high yielding reaction mediated by fully achiral components, we began to test the feasibility of asymmetric hydrogenation with a commercially available chiral thiol: a

Scheme 5. Screen of prochiral substrates under original conditions

"Percent conversion determined by <sup>1</sup>H NMR as the crude ratio of starting material to product peaks. <sup>b</sup>Percent conversion determined by GC-FID as the crude ratio of starting material to product peaks.

Table 1. Initial optimization of metal catalyst

Entry	Time (h)	Metal Catalyst	Loading (mol%)	Conversion to Product (%) <sup>a</sup>
1	24	Fe(acac) <sub>3</sub>	10	93
2	41	Co(salen)	10	35
3	41	Mn(dpm) <sub>3</sub>	10	7
4	24	Fe(acac) <sub>3</sub>	15	98
5 <sup>b</sup>	24	Fe(acac) <sub>3</sub>	15	97

<sup>a</sup>Percent conversion determined by GC-FID as the crude ratio of starting material to product peaks. <sup>b</sup>Reaction concentration 0.2 M.

thioglycoside utilized by Roberts and coworkers (C1).  $^{20a,30}$  The current conditions (Table 2, entry 1) afforded a high yield but minimal enantioinduction. A number of variations led to alteration of the reaction efficiency but no enhanced enantioselectivity. For example, moderate heating to 50 °C led to lower yield and nearly racemic

Table 2. Solvent screen for enantioselectivity

95:5 THF:EtOH 95:5 Benzene:EtOH

95:5 Dioxane:EtOH

95:5 Dioxane: PrOH

6 7<sup>d</sup>

37

51

37

59:41

57:43

61:39

55.5:44.5

nd = not determined. "Percent conversion determined by GC-FID as the crude ratio of starting material to product peaks. <sup>b</sup>Enantiomeric ratio (er) determined by HPLC with a chiral stationary phase. Peaks reported in order of elution. 'Reaction temperature 50 °C. <sup>d</sup>Reaction time 72 h.

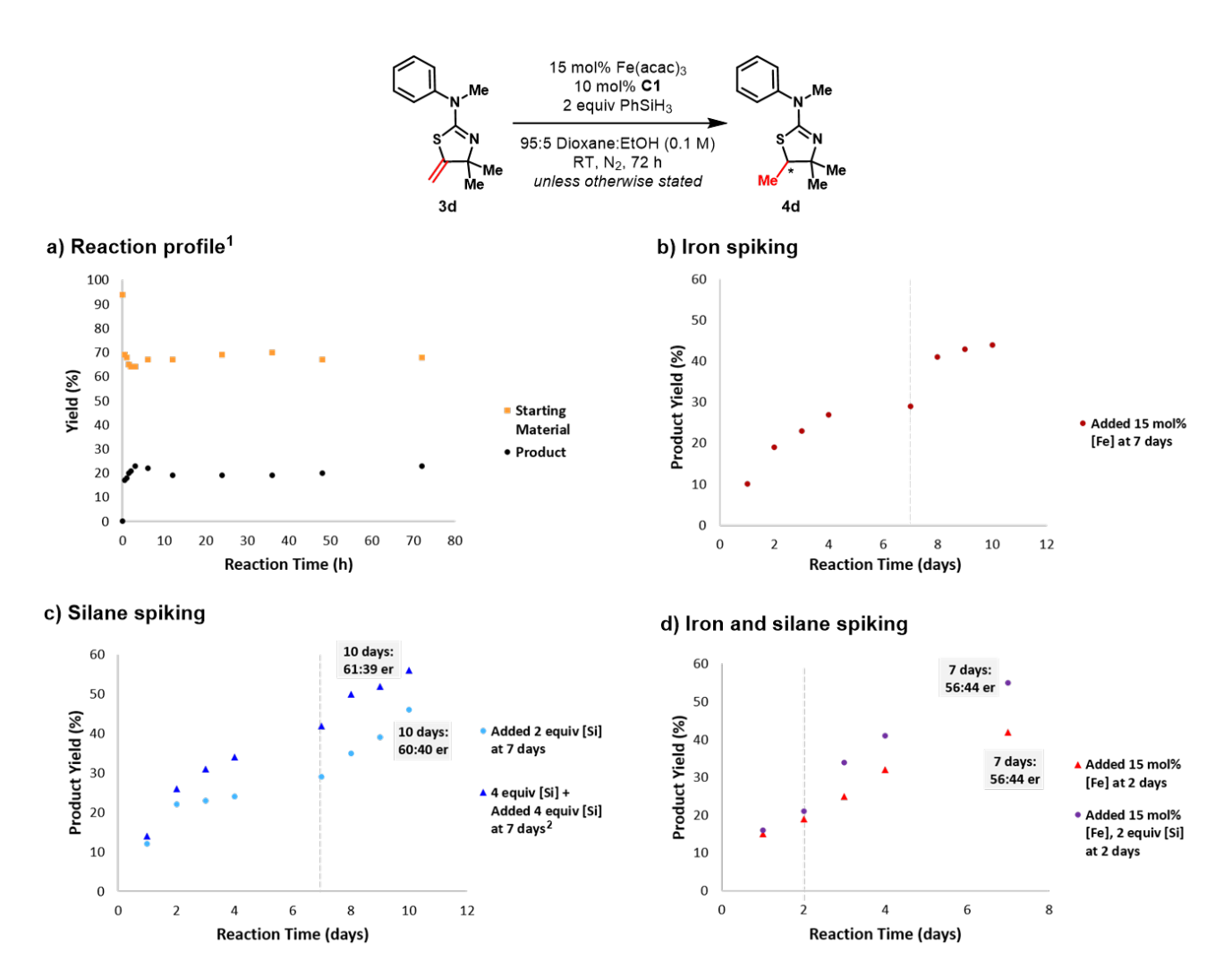


Figure 3. Reaction profile and spiking of iron and silane. Percent yield determined by GC-FID with a calibration curve. ¹Reaction run with 7.5 mol% [Fe¹II(acac)<sub>2</sub>(μ-OEt)]<sub>2</sub>. ²Reaction was initially set up with 4 equiv PhSiH<sub>3</sub>. An additional 4 equiv PhSiH<sub>3</sub> was added at 7 days.

product (Table 2, entry 2). Changing the EtOH solvent to *i*PrOH similarly decreased reaction efficiency (Table 2, entry 3).

We hypothesized that pure alcohol solvents may disrupt noncovalent interactions between substrate and thiol catalysts, prompting us to explore solvent mixtures that contained nonpolar co-solvents (Table 2, entries 4–7). These changes enabled us to observe unambiguous enantioinduction for the first time (61:39 er), with the highest er obtained in 95:5 dioxane:EtOH mixture (Table 2, entry 6). Additional screening is presented in the SI.

Mechanistic Insights Into the Asymmetric Reaction. Mechanism-driven experiments allowed us to improve the yield of olefin hydrogenation to 74% yield in  $24\,h$  (improved from the original 26% yield in  $72\,h$ ), while the er of 61:39 was retained. These studies are presented in Figure 3.

Figure 3a shows the reaction progress versus time for the reaction conditions listed in the equation. Notably, the majority of the conversion took place in the first 12–24 hours, at which point the reaction rate decreased. The loss of mass balance over time is minimal and consistent throughout the reaction. This behavior is characteristic of catalyst deactivation, as described above from mechanistic studies of the achiral reaction. We additionally monitored er over time, and found that the enantioselectivity was consistent over the course of the reaction (see SI). In the remainder of the studies, mass

balance remains satisfactory, so we focus our attention on product formation and er only.

We next sought to investigate iron, silane, and thiol as possible sources of the deactivation when employing a chiral thiol catalyst. We began by spiking the reaction with additional iron catalyst (Figure 3b) to test if the reaction would reinitiate after deactivation. We allowed the initial reaction to proceed for 7 days to ensure complete rate drop off, then added an extra 15 mol% of solid Fe(acac)<sub>3</sub> (indicated by the light gray line on Figure 3b) and monitored the reaction further. The reaction rate increased after the iron spiking, giving increased overall yield. However, this rate increase is short lived and once again dwindles, further supporting iron deactivation as a main source of the decreasing rate.

Next, we added additional silane during the catalytic reaction, through two separate experiments as defined in Figure 3c. Each addition led to increases in reaction rate and yield, implying that silane decomposition is also occurring. We further observed no reduction of er.

We then repeated the iron spiking on a shorter timescale adding 15 mol% Fe(acac)<sub>3</sub> at two days and observed lower er (Figure 3d). Finally, we found the observed effects on yield and er were additive when both iron and silane were spiked together. Our individual spiking observations hold true in the combined case; enantioinduction

is not impacted by extra silane, but is reduced in the presence of extra iron, regardless of whether extra silane is added simultaneously.

We hypothesize that higher concentrations of iron may increase the rate of the racemic background iron-only reactivity excluding thiol, in analogy to Shenvi and Herzon's hydrogenation systems, <sup>8e, f</sup> resulting in the observed degradation of er. Overall, the various spiking studies support the possibility of catalyst deactivation arising from both iron and silane, a result consistent with the kinetic results above. However, the yield increase from spiking is only moderate even when carried out for both iron catalyst and silane. Additional spiking and loading studies are available in the SI.

Additionally, since disulfide is present under catalytic conditions as a result of catalyst deactivation (see above), we chose to test the competency of disulfides themselves as cataly sts or precatalysts. Employing achiral disulfides, we found comparable yields between PhSH and PhSSPh (Scheme 6, see SI for other tests). Given that the reaction is generally under reductive conditions, it is plausible that any disulfides (pre-formed or made *in situ*) can be reduced to their active free thiol in solution. Therefore, we conclude the formation of disulfides in the catalytic reaction is not a major source of catalyst deactivation or sequestration.

**Modulation of Enantioselectivity.** We then turned our attention to screening a variety of chiral thiols derived from both peptides and carbohydrates to supplement our initial examination of **C1** (Table 3, entry 1). With peptide-derived catalysts, the thiol source was primarily derived from incorporation of cysteine (Table 3, entries 2-4). Unfortunately, these cysteine catalysts provided minimal enantioinduction. Based on our previous finding that achiral disulfides

Scheme 6. Testing disulfide in the reaction<sup>a</sup>

with 10 mol% PhSH: 66% yield with 5 mol% PhSSPh: 78% yield

were competent precatalysts, we compared a corresponding chiral disulfide/free thiol pair (Table 3, entries 4-5). Chiral disulfide **C5** does generate product, a finding which agrees with our mechanistic work utilizing disulfides in the racemic system, but with reduced yields and minimal enantioinduction. We also tested a peptide containing an aromatic thiol (**C6**) rather than a cysteine, given its increased similarity to PhSH; however, it did not furnish appreciable enantioinduction (Table 3, entry 6). Additional screening of other peptide catalysts and chiral ligands is available in the SI.

Based on our early observation of enantioselectivity with C1, we wondered if alternate carbohydrate thiol catalysts would provide enhancement in er (Table 3, entries 7-9). We synthesized C7 with the hypothesis that utilizing a bulkier protecting group on the sugar backbone may lead to increased enantioinduction; however, we observed no change in er (Table 3, entry 7). Utilizing a galactose backbone (C8) instead resulted in a minor erosion of er (Table 3, entry 8). Finally, the structurally dissimilar furanose catalyst C9 provided slightly increased enantioinduction, but with a reversal of observed selectivity (Table 3, entry 9). Given the similarity of the results, we

continued with C1 for method development based on its commercial availability and ease of handling.

Guided by the mechanistic insights described above, we performed additional screening of the asymmetric system in reference to the previous best result (Table 4, entry 1). First, we tested whether a more sterically demanding ligand could prevent catalyst deactivation by slowing down steps **A** and **B** of Scheme 4. Ligands were selected based upon previous reports by Baran and coworkers.<sup>33</sup> Similar to Baran's observations, we observed a balance between steric demands and reactivity. While both Fe(dpm)<sub>3</sub> and Fe(dibm)<sub>3</sub>

Table 3. Testing chiral thiols

Entry	Chiral Thiol	Yield (%) <sup>a</sup>	er <sup>b</sup>	
1	C1	26	61:39	
2 3 4 5 6 7 8 9	Boc-Cys-OMe (C2) Boc-Cys- <sup>D</sup> Pro-Acpc-Phg-NMe <sub>2</sub> (C3) Boc-Cys- <sup>D</sup> Pro-Aib-Phe-Pip (C4) [Boc-Cys- <sup>D</sup> Pro-Aib-Phe-Pip] <sub>2</sub> (C5) 2-thio-Bz- <sup>D</sup> Pro-Acpc-Cha-NMe <sub>2</sub> (C6) C7 C8 C9	48 16 45 12 51 31 29 35	51:49 49:51 47:53 49:51 48:52 61:39 58:42 37:63	

Acpc = 1-aminocyclopropane-1-carboxylic acid, Aib = 2-aminoisobutyric acid, Cha = cyclohexylalanine, Phg = phenylglycine, Pip = piperidine. "Percent yield determined by GC-FID with a calibration curve. bEnantiomeric ratio (er) determined by HPLC with a chiral stationary phase. Peaks reported in order of elution. "Reaction was run with 7.5 mol% [Fe<sup>III</sup>(acac)<sub>2</sub>( $\mu$ -OEt)]<sub>2</sub> dPercent conversion determined by GC-FID as the crude ratio of starting material to product peaks.

<sup>&</sup>lt;sup>a</sup> Percent yield determined by GC-FID with a calibration curve.

Table 4. Final optimization of the asymmetric system

Entry	[Fe]	Silane	Solvent	Time (h)	Yield (%)ª	er
1	Fe(acac) <sub>3</sub>	PhSiH <sub>3</sub>	dioxane	72	26	61:39
2 3 4 5 6	Fe(dpm) <sub>3</sub> Fe(dibm) <sub>3</sub> Fe(dibm) <sub>3</sub> Fe(acac) <sub>3</sub> Fe(dibm) <sub>3</sub>	PhSiH <sub>3</sub> PhSiH <sub>3</sub> PhSi(O <i>i</i> Pr)H <sub>2</sub> PhSiH <sub>3</sub> PhSi(O <i>i</i> Pr)H <sub>2</sub>	MTBE	72 72 24 72 24	39 38 63 65 74	60:40 63.5:36.5 58.5:41.5 60:40 61:39

"Percent yield determined by GC-FID with a calibration curve. <sup>b</sup>Enantiomeric ratio (er) determined by HPLC with a chiral stationary phase. Peaks reported in order of elution.

increased yield,  $Fe(dibm)_3$  additionally provided a slight boost in enantioinduction (Table 4, entries 2-3). This result indicates that iron may be involved in the enantiodetermining step, which is consistent with our earlier hypothesis that it is an iron–thiol complex that engages the transient radical. See SI for additional optimization of the metal catalyst.

Next, we considered the choice of silane. As in the mechanistic studies of the racemic reaction, changing to PhSi(OiPr)H<sub>2</sub> improved the asymmetric method to increase both yield and rate (Table 4, entry 3 vs 4). A variety of other silanes provided minimal to no conversion (see SI). Additionally, we tested methyl *tert*-butyl ether (MTBE) and observed a boost in yield of formation of **4d** (Table 4, entry 5). The effects of all three changes were additive, with the highest yield resulting from Fe(dibm)<sub>3</sub>, PhSi(OiPr)H<sub>2</sub>, and MTBE with no significant change in er (Table 4, entry 6). We moved forward with these reaction conditions for an assessment of the impact of variations to the substrate on the overall reaction efficiency and selectivity.

We also evaluated the internal olefin presented in Table 5, conscious of the possible impact of trisubstitution on the reaction selectivity. Gratifyingly, we observed a significant level of enantioselectivity (25:75 er) for the hydrogenation upon changing the ligand from acacH to dibmH. This further supports the hypothesis that iron is present in the enantiodetermining step (H-atom transfer from an iron(II) thiol complex). A change of the solvent system to 95:5 MTBE:EtOH led to a shorter reaction time and higher er, the latter of which is consistent with our spectroscopic studies indicating that iron(II) thiol binding may be more favorable in less polar solvents. Additionally, we screened the alternate carbohydrate-derived thiols using the internal olefin and found similar trends, with the highest er still provided by C1 (see SI).

Having identified a chiral thiol catalyst, **C1**, and optimized reaction conditions that led to observation of meaningful er values, we assessed the mutual influences of different substrate features on selectivity with a number of prochiral substrates (Scheme 7). Namely,

Table 5. Screening conditions for internal olefin

Entry	[Fe]	Sllane	Solvent	Time	Yield (%) <sup>a</sup>	er <sup>b</sup>
1°		PhSiH <sub>3</sub>	dioxane	7 days	10	37.5:62.5
2		PhSi(O <i>i</i> Pr)H <sub>2</sub>	dioxane	72 h	10	30:70
3		PhSi(O <i>i</i> Pr)H <sub>2</sub>	MTBE	24 h	13	25:75

"Percent yield determined by GC-FID with a calibration curve. <sup>b</sup>Enantiomeric ratio (er) determined by HPLC with a chiral stationary phase. Peaks reported in order of elution. Percent conversion to product determined by GC-FID as the crude ratio of starting material to product peaks.

we tested a variety of thiazolidines as well as two cyclic ureas, with assorted functional groups and substituents of differing steric demand. In general, we examined two sets of conditions as defined in Scheme 7. In Conditions A, we used  $Fe(acac)_3$ ,  $PhSiH_3$ , and dioxane, whereas in Conditions B, we used  $Fe(dibm)_3$ ,  $PhSi(OiPr)H_2$ , and MTBE as defined by the mechanistically-guided optimization. We found that Conditions B resulted in a near-uniform yield increase across substrates and similar-to-increased er, in comparison to original Conditions A. These improvements highlight the ability of our mechanistic investigations to improve the enantioselective catalysis.

The minimal enantioinduction afforded by the free methylene and terminal olefin of **3f** (**4f**, 48:52 er) highlights that a fully substituted center adjacent to the olefin is necessary for notable enantioselectivity. In contrast to 3f, unambiguous selectivity was observed for both fully substituted products 4d (61:39 er) and 4g (37.5:62.5 er). We further observe increased net enantioinduction when comparing the dimethyl-substituted thiazolidine (4e, 25:75 er) to the slightly bulkier spirocyclohexane (4h, 80:20 er), though the effect is modest. The most significant variable is the steric bulk from an internal olefin, evidenced by 3e (producing 4e, 25:75 er) and 3h (producing 4h, 80:20 er) exhibiting the highest enantioselectivity of all the tested substrates. Unfortunately, these bulky substrates also provided the lowest yields, and additional optimization would be required to increase the synthetic utility in these cases. Overall, the enantioinduction is influenced strongly by steric effects for this hydrogenation system.

Results with a number of other substrates (products **4b**, **4c**, **4i**, **4j**, **4k**, **4l**) are also presented in Scheme 7. These examples reveal a range of yields and er values that could provide starting points for future optimization with the compatibility of cHAT with Fe-based catalysis now firmly established.

There are limitations, as shown by two substrates that did not result in desired product formation under the reaction conditions.

Conditions A: Fe(acac)<sub>3</sub>, PhSiH<sub>3</sub>, dioxane, 72 h Conditions B: Fe(dibm)<sub>3</sub>, PhSi(O*i*Pr)H<sub>2</sub>, MTBE, 24 h

"Percent yield determined by GC-FID with a calibration curve. "Enantiomeric ratio (er) determined by HPLC with a chiral stationary phase. Peaks reported in order of elution. "Reaction solvent: 95:5 benzene:EtOH. Enantiomeric ratio (er) determined by GC-FID with a chiral stationary phase. Peaks reported in order of elution. "Percent conversion to product determined by GC-FID as the crude ratio of starting material to product peaks. "Reaction time 7 h. "Reaction time 7 days. "Yield determined by 1H NMR with 1,2,4,5-tetramethylbenzene as the internal standard."

Substrate **3m** contains a nitro group that is likely to be reduced under our reaction conditions as observed in similar mHAT reaction conditions.<sup>34</sup> By contrast, **3n** led to only recovered starting material, which we tentatively attribute to the incompatibility of the *N*-benzyl substituent noted above in Scheme 5.

#### **CONCLUSIONS**

Here, mechanistic studies have been employed to advance the hydrogenation of unactivated olefins via cHAT. The compatibility of chiral thiol catalysts with these Fe-catalyzed reactions is a central finding, supported by the first observations of appreciable enantioinduction by iron-based catalysts under mHAT conditions. Kinetic studies of the reaction employing achiral catalysts show that the rate is zero-order with respect to all reagents except silane. Solvolysis studies with PhSi(OiPr)H2 suggest that PhSi(OEt)H2 is faster in the hydrogenation reaction than PhSi(OiPr)H<sub>2</sub>. These both indicate that formation of the [Fe<sup>III</sup>]-H intermediate is the turnover limiting step, and the pseudo-zero order dependence on iron concentration may be explained by the observed catalyst deactivation. From our kinetic studies, spectroscopic work, and computations, we propose a mechanism for cHAT that includes iron(II) thiol binding and transfer of H atom from the iron-bound thiol to the alkyl radical for PCET delivery of the second hydrogen atom in the enantiodetermining step. This forms an iron(III)-thiolate intermediate, which was observed by Mössbauer spectroscopy. We used these insights to explore the asymmetric hydrogenation of thiazolidines containing prochiral olefins, employing a commercially available glucose-derived chiral thiol catalyst. The mechanistic exploration of this system guided our choice of nonpolar solvent mixtures, bulkier ligands, and a more reactive silane to ultimately enhance the yield, rate, and er in several cases. Exploration of the substrate scope suggests that the degree of enantioinduction is substrate-dependent and is more sensitive to steric environment than to non-covalent interactions.

This work adds to the small but growing number of asymmetric mHAT reactions enabled by small-molecule catalysts, and provides, to the best of our knowledge, the first demonstration of asymmetric hydrogenation via iron-catalyzed mHAT. Further, it shows the potential for cooperative reactivity between iron and thiols. The compatibility of chiral thiol catalysts with these Fe-catalyzed reactions creates an exciting opportunity for the development of novel asymmetric iron-catalyzed mHAT reactions.

#### **ASSOCIATED CONTENT**

## **Supporting Information**

The supporting information is available free of charge on the ACS Publications website.

Synthetic procedures, experimental details, kinetic data, spectroscopic data, characterization data, NMR spectra, chiral HPLC chromatograms, X-ray crystallographic data, computational details, and additional screening results (PDF)

Raw data (ZIP) X-ray data for **3c**, **3g**, **3h**, **3k**, and **3l** (CIF)

#### **Accession Codes**

CCDC 2304692–2304696 contain the supplementary crystallographic data for this paper. These data can be obtained free of charge via www.ccdc.cam.ac.uk/data\_request/cif, or by emailing data\_request@ccdc.cam.ac.uk, or by contacting The Cambridge Crystallographic Data Centre, 12 Union Road, Cambridge CB2 1EZ, UK; fax: +44 1223 336033.

#### **AUTHOR INFORMATION**

#### **Corresponding Authors**

\* Patrick L. Holland - Department of Chemistry, Yale University, New Haven, Connecticut 06520, United States;

Email: patrick.holland@yale.edu

\* Scott J. Miller – Department of Chemistry, Yale University, New Haven, Connecticut 06520, United States; Email: scott.miller@yale.edu
\* Julian G. West – Department of Chemistry, Rice University, BioScience Research Collaborative, Houston, Texas 77030, United States; Email: jgwest@rice.edu

#### **ORCID**

Patrick L. Holland: https://orcid.org/0000-0002-2883-2031
Scott J. Miller: https://orcid.org/0000-0001-7817-1318
Julian G. West: http://orcid.org/0000-0002-3715-7883
Jolie Kan: https://orcid.org/0009-0005-6473-0189
Dinora N. Rodriguez: https://orcid.org/0000-0001-6524-547X
Juan M. I. Serviano: https://orcid.org/0009-0009-4616-8750
Padmanabha V. Kattamuri: https://orcid.org/0000-0002-5381-1347
Savannah M. Mason: https://orcid.org/0009-0005-7470-4654
Sarah R. Buzsaki: https://orcid.org/0000-0001-8398-0494

## **Author Contributions**

All authors have given approval to the final version of the manuscript. <sup>‡</sup> These authors contributed equally and each has the right to list themselves first in author order on their CVs.

## **Funding Sources**

Funding for this work was provided by the NIH (GM-129081 to P. L. H., GM-132092 to S. J. M., GM142738 to J. G. W.), CPRIT (RR190025 to J. G. W. and RR220055 for D.N.R.), Welch Foundation (C-2085 to J. G. W.), and NSF RLEAD REU (CHE 2150216 to J. K.).

#### Notes

The authors declare no competing financial interest.

#### **ACKNOWLEDGMENT**

Funding for this work was provided by the NIH (GM-129081 to P. L. H., GM-132092 to S. J. M., GM142738 to J. G. W.), CPRIT (RR190025 and RR220055 to J. G. W. and RR220055 for D.N.R.), Welch Foundation (C-2085 to J. G. W.), and NSF RLEAD REU (CHE 2150216 to J. K.). We thank Dr. Jonathan Ryss and Marcus Vinicius Pinto Pereira Junior for sharing peptide catalysts. Thank you to Dr. Reagan Hooper for guidance with computations. We acknowledge the Yale Center for

Research Computing for use of the research computing infrastructure. We acknowledge the Shared Equipment Authority of Rice University for use of the X-ray Facilities and Mass Spectrometer Facilities. This work made use of the Chemical and Biophysical Instrumentation Center at Yale University.

#### **REFERENCES**

- (1) (a) Knowles, W. S. Asymmetric Hydrogenations (Nobel Lecture). Angew. Chem. Int. Ed. 2002, 41, 1998-2007. DOI: 10.1002/1521-3773(20020617)41:12<1998::AID-ANIE1998>3.0.CO;2-8. (b) Noyori, R. Asymmetric Catalysis: Science and Opportunities (Nobel Lecture). Angew. Chem. Int. Ed. 2002, 41, 2008-2022. DOI: 10.1002/1521-3773(20020617)41:12<2008::AID-ANIE2008>3.0.CO;2-4. (c) Lennon, I. C.; Pilkington, C. J. The Application of Asymmetric Hydrogenation for the Manufacture of Pharmaceutical Intermediates: The Need for Catalyst Diversity. Synthesis 2003, 2003, 1639-1642. DOI: 10.1055/s-2003-40871. (d) Shimizu, H.; Nagasaki, I.; Matsumura, K.; Sayo, N.; Saito, T. Developments in Asymmetric Hydrogenation from an Industrial Perspective. Acc. Chem. Res. 2007, 40, 1385-1393. DOI: 10.1021/ar700101x. (e) Johnson, N. B.; Lennon, I. C.; Moran, P. H.; Ramsden, J. A. Industrial-Scale Synthesis and Applications of Asymmetric Hydrogenation Catalysts. Acc. Chem. Res. 2007, 40, 1291-1299. DOI: 10.1021/ar700114k. (f) Woodmansee, D. H.; Pfaltz, A. Iridium-Catalyzed Asymmetric Hydrogenation of Olefins with Chiral N,P and C,N Ligands. In Iridium Catalysis, Andersson, P. G. Ed.; Springer Berlin Heidelberg, 2011; pp 31-76. (g) Blaser, H.-U.; Pugin, B.; Spindler, F. Asymmetric Hydrogenation. In Organometallics as Catalysts in the Fine Chemical Industry, Beller, M., Blaser, H.-U. Eds.; Springer Berlin Heidelberg, 2012; pp 65-102.
- (2) (a) Horiuti, I.; Polanyi, M. Exchange reactions of hydrogen on metallic catalysts. *Trans. Faraday Soc.* **1934**, *30*, 1164-1172. DOI: 10.1039/TF9343001164. (b) Bond, G. C.; Wells, P. B. The Mechanism of the Hydrogenation of Unsaturated Hydrocarbons on Transition Metal Catalysts. In *Advances in Catalysis*, Eley, D. D., Pines, H., Weisz, P. B. Eds.; Vol. 15; Academic Press, 1965; pp 91-226. (c) Zaera, F. Key unanswered questions about the mechanism of olefin hydrogenation catalysis by transition-metal surfaces: a surface-science perspective. *Phys. Chem. Chem. Phys.* **2013**, *15*, 11988-12003. DOI: 10.1039/C3CP50402F. (d) Blaser, H. U.; Pugin, B.; Spindler, F.; Saudan, L. A. Hydrogenation. In *Applied Homogeneous Catalysis with Organometallic Compounds*, 2017; pp 621-690.
- (3) (a) Halpern, J. Mechanism and Stereoselectivity of Asymmetric Hydrogenation. Science 1982, 217, 401-407. (b) Knowles, W. S. Asymmetric hydrogenation. Acc. Chem. Res. 1983, 16, 106-112. DOI: 10.1021/ar00087a006. (c) Gridnev, Ilya D.; Yamanoi, Y.; Higashi, N.; Tsuruta, H.; Yasutake, M.; Imamoto, T. Asymmetric Hydrogenation Catalyzed by (S,S)-R-BisPast;-Rh and (R,R)-R-MiniPHOS Complexes: Scope, Limitations, and Mechanism. Adv. Synth. Catal. 2001, 343, 118-136. 10.1002/1615-4169(20010129)343:1<118::AID-ADSC118>3.0.CO;2-Z. (d) Källström, K.; Munslow, I.; Andersson, P. G. Ir-Catalysed Asymmetric Hydrogenation: Ligands, Substrates and Mechanism. Chem. Eur. J. 2006, 12, 3194-3200. DOI: 10.1002/chem.200500755. (e) Imamoto, T. Asymmetric Hydrogenation. In Hydrogenation, Iyad, K. Ed.; IntechOpen, 2012; p Ch. 1. (f) Seo, C. S. G.; Morris, R. H. Catalytic Homogeneous Asymmetric Hydrogenation: Successes and Opportunities. Organometallics 2019, 38, 47-65. DOI: 10.1021/acs.organomet.8b00774. (g) Behera, P.; Ramakrishna, D. S.; Chandrasekhar, M. M.; Kothakapu, S. R. A concise review on recent advances in catalytic asymmetric hydrogenation. Chirality 2023, 35, 477-497. DOI: 10.1002/chir.23559.
- (4) (a) Broene, R. D.; Buchwald, S. L. Asymmetric hydrogenation of unfunctionalized trisubstituted olefins with a chiral titanocene catalyst. *J. Am. Chem. Soc.* **1993**, *115*, 12569-12570. DOI: 10.1021/ja00079a040. (b) Ohta, T.; Ikegami, H.; Miyake, T.; Takaya, H. BINAP-Ru(II) and BINAP-Rh(I)-catalyzed asymmetric hydrogenation of olefins without heteroatom-functionalities. *J. Organomet. Chem.* **1995**, *502*, 169-176. DOI: 10.1016/0022-328X(95)05819-B. (c) Schmid, R.; Broger, E. A.; Cereghetti, M.; Crameri, Y.; Foricher, J.; Lalonde, M.; Müller, R. K.; Scalone, M.; Schoettel, G.; Zutter, U. New developments in enantioselective

hydrogenation. Pure Appl. Chem. 1996, 68, 131-138. DOI: 10.1351/pac199668010131. (d) Lightfoot, A.; Schnider, P.; Pfaltz, A. Enantioselective Hydrogenation of Olefins with Iridium-Phosphanodihydrooxazole Catalysts. Angew. Chem. Int. Ed. 1998, 37, 2897-2899. DOI: 10.1002/(SICI)1521-3773(19981102)37:20<2897::AID-ANIE2897>3.0.CO;2-8. (e) Forman, G. S.; Ohkuma, T.; Hems, W. P.; Noyori, R. Asymmetric hydrogenation of α-ethylstyrenes catalyzed by chiral ruthenium complexes. Tetrahedron Lett. 2000, 41, 9471-9475. DOI: 10.1016/S0040-4039(00)01613-0. (f) Pfaltz, A.; Blankenstein, J.; Hilgraf, R.; Hörmann, E.; McIntyre, S.; Menges, F.; Schönleber, M.; Smidt, S. P.; Wüstenberg, B.; Zimmermann, N. Iridium-Catalyzed Enantioselective Hydrogenation of Olefins. Adv. Synth. Catal. 2003, 345, 33-43. DOI: 10.1002/adsc.200390027. (g) Cui, X.; Burgess, K. Catalytic Homogeneous Asymmetric Hydrogenations of Largely Unfunctionalized Alkenes. Chem. Rev. 2005, 105, 3272-3296. DOI: 10.1021/cr0500131. (h) Roseblade, S. J.; Pfaltz, A. Iridium-Catalyzed Asymmetric Hydrogenation of Olefins. Acc. Chem. Res. 2007, 40, 1402-1411. DOI: 10.1021/ar700113g.

(5) (a) Zhang, Z.; Butt, N. A.; Zhou, M.; Liu, D.; Zhang, W. Asymmetric Transfer and Pressure Hydrogenation with Earth-Abundant Transition Metal Catalysts. *Chin. J. Chem* . **2018**, 36, 443-454. DOI: 10.1002/cjoc.201800053. (b) Pellissier, H. Recent developments in enantioselective cobalt-catalyzed transformations. *Coord. Chem. Rev.* **2018**, 360, 122-168. DOI: 10.1016/j.ccr.2018.01.013. (c) Wen, J.; Wang, F.; Zhang, X. Asymmetric hydrogenation catalyzed by first-row transition metal complexes. *Chem. Soc. Rev.* **2021**, 50, 3211-3237. DOI: 10.1039/DOCS00082E.

(6) (a) Mazuela, J.; Pàmies, O.; Diéguez, M. Expanded Scope of the Asymmetric Hydrogenation of Minimally Functionalized Olefins Catalyzed by Iridium Complexes with Phosphite-Thiazoline Ligands. ChemCatChem 2013, 5, 2410-2417. DOI: 10.1002/cctc.201300189. (b) Kraft, S.; Ryan, K.; Kargbo, R. B. Recent Advances in Asymmetric Hydrogenation of Tetrasubstituted Olefins. J. Am. Chem. Soc. 2017, 139, 11630-11641. DOI: 10.1021/jacs.7b07188. (c) Margarita, C.; Andersson, P. G. Evolution and Prospects of the Asymmetric Hydrogenation of Unfunctionalized Olefins. J. Am. Chem. Soc. 2017, 139, 1346-1356. DOI: 10.1021/jacs.6b10690. (d) Meemken, F.; Baiker, A. Recent Progress in Heterogeneous Asymmetric Hydrogenation of C=O and C=C Bonds on Supported Noble Metal Chem. Rev. **2017**, 117, 11522-11569. 10.1021/acs.chemrev.7b00272. (e) Biosca, M.; Magre, M.; Pàmies, O.; Diéguez, M. Asymmetric Hydrogenation of Disubstituted, Trisubstituted, and Tetrasubstituted Minimally Functionalized Olefins and Cyclic  $\beta$ -Enamides with Easily Accessible Ir-P, Oxazoline Catalysts. ACS Catal. 2018, 8, 10316-10320. DOI: 10.1021/acscatal.8b03170. (f) Lu, P.; Wang, H.; Mao, Y.; Hong, X.; Lu, Z. Cobalt-Catalyzed Enantioconvergent Hydrogenation of Minimally Functionalized Isomeric Olefins. J. Am. Chem. Soc. 2022, 144, 17359-17364. DOI: 10.1021/jacs.2c08525.

(7) (a) Sweany, R. L.; Halpern, J. Hydrogenation of α-methylstyrene by hydridopentacarbonylmanganese(I). Evidence for a free-radical mechanism. *J. Am. Chem. Soc.* **1977**, 99, 8335-8337. DOI: 10.1021/ja00467a045. (b) Eisenberg, D. C.; Norton, J. R. Hydrogen-Atom Transfer Reactions of Transition-Metal Hydrides. *Isr. J. Chem.* **1991**, 31, 55-66. DOI: 10.1002/ijch.199100006. (c) Hartung, J.; Norton, J. R. Catalysis Involving the H• Transfer Reactions of First-Row Transition Metals. In *Catalysis without Precious Metals*, 2010; Wiley. pp 1-24. (d) Mayer, J. M. Understanding Hydrogen Atom Transfer: From Bond Strengths to Marcus Theory. *Acc. Chem. Res.* **2011**, 44, 36-46. DOI: 10.1021/ar100093z.

(8) For review: (a) Crossley, S. W. M.; Obradors, C.; Martinez, R. M.; Shenvi, R. A. Mn-, Fe-, and Co-Catalyzed Radical Hydrofunctionalizations of Olefins. Chem. Rev. 2016, 116, 8912-9000. 10.1021/acs.chemrev.6b00334. (b) Shevick, S. L.; Wilson, C. V.; Kotesova, S.; Kim, D.; Holland, P. L.; Shenvi, R. A. Catalytic hydrogen atom transfer to alkenes: a roadmap for metal hydrides and radicals. Chem. Sci. 2020, 11, 12401-12422. DOI: 10.1039/D0SC04112B. (c) Wu, J.; Ma, Z. Metalhydride hydrogen atom transfer (MHAT) reactions in natural product synthesis. Org. Chem. Front. 2021, 8, 7050-7076. DOI: 10.1039/D1QO01139A. Selected examples: (d) Barker, T. J.; Boger, D. L. Fe(III)/NaBH<sub>4</sub>-Mediated Free Radical Hydrofluorination of Unactivated Alkenes. J. Am. Chem. Soc. 2012, 134, 13588-13591. DOI:

10.1021/ja3063716. (e) Iwasaki, K.; Wan, K. K.; Oppedisano, A.; Crossley, S. W. M.; Shenvi, R. A. Simple, Chemoselective Hydrogenation with Thermodynamic Stereocontrol. J. Am. Chem. Soc. 2014, 136, 1300-1303. DOI: 10.1021/ja412342g. (f) King, S. M.; Ma, X.; Herzon, S. B. A Method for the Selective Hydrogenation of Alkenyl Halides to Alkyl Halides. J. Am. Chem. Soc. 2014, 136, 6884-6887. DOI: 10.1021/ja502885c. (g) Lo, J. C.; Yabe, Y.; Baran, P. S. A Practical and Catalytic Reductive Olefin Coupling. J. Am. Chem. Soc. 2014, 136, 1304-1307. DOI: 10.1021/ja4117632. (h) Lo, J. C.; Kim, D.; Pan, C.-M.; Edwards, J. T.; Yabe, Y.; Gui, J.; Qin, T.; Gutiérrez, S.; Giacoboni, J.; Smith, M. W.; Holland, P. L.; Baran, P. S. Fe-Catalyzed C-C Bond Construction from Olefins via Radicals. J. Am. Chem. Soc. 2017, 139, 2484-2503. DOI: 10.1021/jacs.6b13155. (i) Saladrigas, M.; Bosch, C.; Saborit, G. V.; Bonjoch, J.; Bradshaw, B. Radical Cyclization of Alkene-Tethered Ketones Initiated by Hydrogen-Atom Transfer. Angew. Chem. Int. Ed. 2018, 57, 182-186. DOI: 10.1002/anie.201709659. (j) Green, S. A.; Vásquez-Céspedes, S.; Shenvi, R. A. Iron-Nickel Dual-Catalysis: A New Engine for Olefin Functionalization and the Formation of Quaternary Centers. J. Am. Chem. Soc. 2018, 140, 11317-11324. DOI: 10.1021/jacs.8b05868. (k) Saladrigas, M.; Loren, G.; Bonjoch, J.; Bradshaw, B. Hydrogen Atom Transfer (HAT)-Triggered Iron-Catalyzed Intra- and Intermolecular Coupling of Alkenes with Hydrazones: Access to Complex ACSCatal. 2018, 8, 11699-11703. 10.1021/acscatal.8b03794. (1) Tardieu, D.; Desnoyers, M.; Laye, C.; Hazelard, D.; Kern, N.; Compain, P. Stereoselective Synthesis of C,C-Glycosides from exo-Glycals Enabled by Iron-Mediated Hydrogen Atom Lett. 2019, 7262-7267. Transfer. Org. 21, 10.1021/acs.orglett.9b02496. (m) Saladrigas, M.; Bonjoch, J.; Bradshaw, B. Iron Hydride Radical Reductive Alkylation of Unactivated Alkenes. Org. Lett. 2020, 22, 684-688. DOI: 10.1021/acs.orglett.9b04459. For review: (n) van der Puyl, V.; Shenvi, R. A. 2.14 Manganese-, Iron-, and Cobalt-Catalyzed Radical Alkene Hydrofunctionalization. In Science of Synthesis: Base-Metal Catalysis, Vol. 2; Thieme Chemistry, 2023; p 623.

(9) Selected examples: (a) Ishikawa, H.; Colby, D. A.; Boger, D. L. Direct Coupling of Catharanthine and Vindoline to Provide Vinblastine: Total Synthesis of (+)- and ent-(-)-Vinblastine. *J. Am. Chem. Soc.* **2008**, 130, 420-421. DOI: 10.1021/ja078192m. (b) Ishikawa, H.; Colby, D. A.; Seto, S.; Va, P.; Tam, A.; Kakei, H.; Rayl, T. J.; Hwang, I.; Boger, D. L. Total Synthesis of Vinblastine, Vincristine, Related Natural Products, and Key Structural Analogues. J. Am. Chem. Soc. 2009, 131, 4904-4916. DOI: 10.1021/ja809842b. (c) Leggans, E. K.; Barker, T. J.; Duncan, K. K.; Boger, D. L. Iron(III)/NaBH<sub>4</sub>-Mediated Additions to Unactivated Alkenes: Synthesis of Novel 20'-Vinblastine Analogues. Org. Lett. 2012, 14, 1428-1431. DOI: 10.1021/ol300173v. (d) George, D. T.; Kuenstner, E. J.; Pronin, S. V. A Concise Approach to Paxilline Indole Diterpenes. J. Am. Chem. Soc. 2015, 137, 15410-15413. DOI: 10.1021/jacs.5b11129. (e) Zhang, Y.; Xue, Y.; Li, G.; Yuan, H.; Luo, T. Enantioselective synthesis of Iboga alkaloids and vinblastine via rearrangements of quaternary ammoniums. Chem. Sci. 2016, 7, 5530-5536. DOI: 10.1039/C6SC00932H. (f) Qu, Y.; Wang, Z.; Zhang, Z.; Zhang, W.; Huang, J.; Yang, Z. Asymmetric Total Synthesis of (+)-Waihoensene. J. Am. Chem. Soc. 2020, 142, 6511-6515. DOI: 10.1021/jacs.0c02143. (g) Li, J.; Li, F.; King-Smith, E.; Renata, H. Merging chemoenzymatic and radical-based retrosynthetic logic for rapid and modular synthesis of oxidized meroterpenoids. Nat. Chem. 2020, 12, 173-179. DOI: 10.1038/s41557-019-0407-6. (h) Zeng, X.; Shukla, V.; Boger, D. L. Divergent Total Syntheses of (-)-Pseudocopsinine and (-)-Minovincinine. J. Org. Chem. 2020, 85, 14817-14826. DOI: 10.1021/acs.joc.0c02493. (i) Foy, N. J.; Pronin, S. V. Synthesis of Pleuromutilin. J. Am. Chem. Soc. 2022, 144, 10174-10179. DOI: 10.1021/jacs.2c04708. (j) Gan, X.-c.; Kotesova, S.; Castanedo, A.; Green, S. A.; Møller, S. L. B.; Shenvi, R. A. Iron-Catalyzed Hydrobenzylation: Stereoselective Synthesis of (-)-Eugenial C. J. Am. Chem. Soc. 2023, 145, 15714-15720. DOI: 10.1021/jacs.3c05428.

(10) Green, S. A.; Crossley, S. W. M.; Matos, J. L. M.; Vásquez-Céspedes, S.; Shevick, S. L.; Shenvi, R. A. The High Chemofidelity of Metal-Catalyzed Hydrogen Atom Transfer. *Acc. Chem. Res.* **2018**, *51*, 2628-2640. DOI: 10.1021/acs.accounts.8b00337.

(11) (a) Liu, H.; Gu, L.; Zhu, P.; Liu, Z.; Zhou, B. Evaluation on Thermal Hazard of Ter-Butyl Hydroperoxide by Using Accelerating Rate

- Calorimeter. *Procedia Eng.* **2012**, 45, 574-579. DOI: 10.1016/j.proeng.2012.08.206. (b) Li, B.; Guinness, S. M.; Hoagland, S.; Fichtner, M.; Kim, H.; Li, S.; Maguire, R. J.; McWilliams, J. C.; Mustakis, J.; Raggon, J.; Campos, D.; Voss, C. R.; Sohodski, E.; Feyock, B.; Murnen, H.; Gonzalez, M.; Johnson, M.; Lu, J.; Feng, X.; Sun, X.; Zheng, S.; Wu, B. Continuous Production of Anhydrous tert-Butyl Hydroperoxide in Nonane Using Membrane Pervaporation and Its Application in Flow Oxidation of a γ-Butyrolactam. *Org. Process Res. Dev.* **2018**, 22, 707-720. DOI: 10.1021/acs.oprd.8b00083.
- (12) Kattamuri, P. V.; West, J. G. Hydrogenation of Alkenes via Cooperative Hydrogen Atom Transfer. *J. Am. Chem. Soc.* **2020**, *142*, 19316-19326. DOI: 10.1021/jacs.0c09544.
- (13) (a) Discolo, C. A.; Touney, E. E.; Pronin, S. V. Catalytic Asymmetric Radical–Polar Crossover Hydroalkoxylation. *J. Am. Chem. Soc.* **2019**, *141*, 17527-17532. DOI: 10.1021/jacs.9b10645. (b) Ebisawa, K.; Izumi, K.; Ooka, Y.; Kato, H.; Kanazawa, S.; Komatsu, S.; Nishi, E.; Shigehisa, H. Catalyst- and Silane-Controlled Enantioselective Hydrofunctionalization of Alkenes by Cobalt-Catalyzed Hydrogen Atom Transfer and Radical-Polar Crossover. *J. Am. Chem. Soc.* **2020**, *142*, 13481-13490. DOI: 10.1021/jacs.0c05017. *For review:* (c) Kennemur, J. L.; Maji, R.; Scharf, M. J.; List, B. Catalytic Asymmetric Hydroalkoxylation of C–C Multiple Bonds. *Chem. Rev.* **2021**, *121*, 14649-14681. DOI: 10.1021/acs.chemrev.1c00620.
- (14) Qin, T.; Lv, G.; Miao, H.; Guan, M.; Xu, C.; Zhang, G.; Xiong, T.; Zhang, Q. Cobalt-Catalyzed Asymmetric Alkylation of (Hetero)Arenes with Styrenes. *Angew. Chem. Int. Ed.* **2022**, *61*, e202201967. DOI: 10.1002/anie.202201967.
- (15) (a) Shen, X.; Chen, X.; Chen, J.; Sun, Y.; Cheng, Z.; Lu, Z. Ligand-promoted cobalt-catalyzed radical hydroamination of alkenes. *Nat. Commun.* **2020**, *11*, 783. DOI: 10.1038/s41467-020-14459-x. (b) Qin, T.; Lv, G.; Meng, Q.; Zhang, G.; Xiong, T.; Zhang, Q. Cobalt-Catalyzed Radical Hydroamination of Alkenes with N-Fluorobenzenesulfonimides. *Angew. Chem. Int. Ed.* **2021**, *60*, 25949-25957. DOI: 10.1002/anie.202110178. (c) Miao, H.; Guan, M.; Xiong, T.; Zhang, G.; Zhang, Q. Cobalt-Catalyzed Enantioselective Hydroamination of Arylalkenes with Secondary Amines. *Angew. Chem. Int. Ed.* **2023**, *62*, e202213913. DOI: 10.1002/anie.202213913. For review: (d) Zhang, G.; Zhang, Q. Cobalt-catalyzed HAT reaction for asymmetric hydrofunctionalization of alkenes and nucleophiles. *Chem. Catal.* **2023**, *3*, 100526. DOI: 10.1016/j.checat.2023.100526.
- (16) Wilson, C. V.; Kim, D.; Sharma, A.; Hooper, R. X.; Poli, R.; Hoffman, B. M.; Holland, P. L. Cobalt–Carbon Bonding in a Salen-Supported Cobalt(IV) Alkyl Complex Postulated in Oxidative MHAT Catalysis. *J. Am. Chem. Soc.* **2022**, 144, 10361-10367. DOI: 10.1021/jacs.2c02128.
- (17) Kim, D.; Rahaman, S. M. W.; Mercado, B. Q.; Poli, R.; Holland, P. L. Roles of Iron Complexes in Catalytic Radical Alkene Cross-Coupling: A Computational and Mechanistic Study. *J. Am. Chem. Soc.* **2019**, *141*, 7473-7485. DOI: 10.1021/jacs.9b02117.
- (18) Wilson, C. V.; Holland, P. L. Mechanism of Alkene Hydrofunctionalization by Oxidative Cobalt(salen) Catalyzed Hydrogen Atom Transfer. *J. Am. Chem. Soc.* **2024**, *146*, 2685-2700. DOI: 10.1021/jacs.3c12329.
- (19) Selected examples: (a) Yahata, K.; Kaneko, Y.; Akai, S. Cobalt-Catalyzed Intermolecular Markovnikov Hydroamination of Nonactivated Olefins: N<sup>2</sup>-Selective Alkylation of Benzotriazole. Org. Lett. 2020, 22, 598-603. DOI: 10.1021/acs.orglett.9b04375. (b) Shigehisa, H.; Aoki, T.; Yamaguchi, S.; Shimizu, N.; Hiroya, K. Hydroalkoxylation of Unactivated Olefins with Carbon Radicals and Carbocation Species as Key Intermediates. J. Am. Chem. Soc. 2013, 135, 10306-10309. DOI: 10.1021/ja405219f. (c) Nagai, T.; Mimata, N.; Terada, Y.; Sebe, C.; Shigehisa, H. Catalytic Dealkylative Synthesis of Cyclic Carbamates and Ureas via Hydrogen Atom Transfer and Radical-Polar Crossover. Org. Lett. 2020, 22, 5522-5527. DOI: 10.1021/acs.orglett.0c01872. (d) Shigehisa, H.; Ano, T.; Honma, H.; Ebisawa, K.; Hiroya, K. Co-Catalyzed Hydroarylation of Unactivated Olefins. Org. Lett. 2016, 18, 3622-3625. DOI: 10.1021/acs.orglett.6b01662. (e) Shigehisa, H.; Hayashi, M.; Ohkawa, H.; Suzuki, T.; Okayasu, H.; Mukai, M.; Yamazaki, A.; Kawai, R.; Kikuchi, H.; Satoh, Y.; Fukuyama, A.; Hiroya, K. Catalytic Synthesis of Saturated Oxygen

- Heterocycles by Hydrofunctionalization of Unactivated Olefins: Unprotected and Protected Strategies. *J. Am. Chem. Soc.* **2016**, *138*, 10597-10604. DOI: 10.1021/jacs.6b05720. (f) Yin, Y.-N.; Ding, R.-Q.; Ouyang, D.-C.; Zhang, Q.; Zhu, R. Highly chemoselective synthesis of hindered amides via cobalt-catalyzed intermolecular oxidative hydroamidation. *Nat. Commun.* **2021**, *12*, 2552. DOI: 10.1038/s41467-021-22373-z. (g) Jana, S.; Mayerhofer, V. J.; Teskey, C. J. Photo- and Electrochemical Cobalt Catalysed Hydrogen Atom Transfer for the Hydrofunctionalisation of Alkenes. *Angew. Chem. Int. Ed.* **2023**, *62*, e202304882. DOI: 10.1002/anie.202304882.
- (20) (a) Haque, M. B.; Roberts, B. P.; Tocher, D. A. Enantioselective radical-chain hydrosilylation of alkenes using homochiral thiols as polarity-reversal catalysts. *J. Chem. Soc., Perkin Trans. 1* **1998**, 2881-2890. DOI: 10.1039/A803280G. (b) Cai, Y.; Roberts, B. P.; Tocher, D. A. Carbohydrate-derived thiols as protic polarity-reversal catalysts for enantioselective radical-chain reactions. *J. Chem. Soc., Perkin Trans. 1* **2002**, 1376-1386. DOI: 10.1039/B202022J.
- (21) (a) Shi, Q.; Xu, M.; Chang, R.; Ramanathan, D.; Peñin, B.; Funes-Ardoiz, I.; Ye, J. Visible-light mediated catalytic asymmetric radical deuteration at non-benzylic positions. *Nat. Commun.* **2022**, *13*, 4453. DOI: 10.1038/s41467-022-32238-8. (b) Ramanathan, D.; Shi, Q.; Xu, M.; Chang, R.; Peñín, B.; Funes-Ardoiz, I.; Ye, J. Catalytic asymmetric deuterosilylation of exocyclic olefins with mannose-derived thiols and deuterium oxide. *Org. Chem. Front.* **2023**, *10*, 1182-1190. DOI: 10.1039/D2Q001979E.
- (22) Shin, N. Y.; Ryss, J. M.; Zhang, X.; Miller, S. J.; Knowles, R. R. Light-driven deracemization enabled by excited-state electron transfer. *Science* **2019**, *366*, *364*-*369*. DOI: doi:10.1126/science.aay2204.
- (23) Hejna, B. G.; Ganley, J. M.; Shao, H.; Tian, H.; Ellefsen, J. D.; Fastuca, N. J.; Houk, K. N.; Miller, S. J.; Knowles, R. R. Catalytic Asymmetric Hydrogen Atom Transfer: Enantioselective Hydroamination of Alkenes. *J. Am. Chem. Soc.* **2023**, *145*, 16118-16129. DOI: 10.1021/jacs.3c04591.
- (24) (a) Burés, J. Variable Time Normalization Analysis: General Graphical Elucidation of Reaction Orders from Concentration Profiles. Angew. Chem. Int. Ed. 2016, 55, 16084-16087. DOI: 10.1002/anie.201609757. (b) Burés, J. What is the Order of a Reaction? Top. Catal. 2017, 60, 631-633. DOI: 10.1007/s11244-017-0735-y. (c) Nielsen, C. D. T.; Burés, J. Visual kinetic analysis. Chem. Sci. 2019, 10, 348-353. DOI: 10.1039/C8SC04698K.
- (25) (a) Blackmond, D. G. Kinetic Profiling of Catalytic Organic Reactions as a Mechanistic Tool. *J. Am. Chem. Soc.* **2015**, *137*, 10852-10866. DOI: 10.1021/jacs.5b05841. (b) Martínez-Carrión, A.; Howlett, M. G.; Alamillo-Ferrer, C.; Clayton, A. D.; Bourne, R. A.; Codina, A.; Vidal-Ferran, A.; Adams, R. W.; Burés, J. Kinetic Treatments for Catalyst Activation and Deactivation Processes based on Variable Time Normalization Analysis. *Angew. Chem. Int. Ed.* **2019**, *58*, 10189-10193. DOI: 10.1002/anie.201903878.
- (26) Obradors, C.; Martinez, R. M.; Shenvi, R. A. Ph(i-PrO)SiH<sub>2</sub>: An Exceptional Reductant for Metal-Catalyzed Hydrogen Atom Transfers. J. Am. Chem. Soc. **2016**, 138, 4962-4971. DOI: 10.1021/jacs.6b02032.
- (27) (a) Hamed, M. Y.; Silver, J.; Wilsonx, M. T. Studies of the reactions of ferric iron with glutathione and some related thiols. *Inorg. Chim. Acta* **1983**, 78, 1-11. DOI: 10.1016/S0020-1693(00)86480-4. (b) Eng, S. J.; Motekaitis, R. J.; Martell, A. E. Degradation of coordinated β-diketonates as iron chelate catalysts during the oxidation of H<sub>2</sub>S to S<sub>8</sub> by molecular oxygen. *Inorg. Chim. Acta* **2000**, 299, 9-15. DOI: 10.1016/S0020-1693(99)00434-X. (c) Hider, R. C.; Kong, X. Iron speciation in the cytosol: an overview. *Dalton Trans.* **2013**, 42, 3220-3229. DOI: 10.1039/C2DT32149A. (d) Paul, S.; Islam, S. M. Oxidative dehydrogenation of thiols to disulfides at room temperature using silica supported iron oxide as an efficient solid catalyst. *RSC Adv.* **2016**, 6, 95753-95759. DOI: 10.1039/C6RA19832E. (e) Kreitman, G. Y.; Danilewicz, J. C.; Jeffery, D. W.; Elias, R. J. Reaction Mechanisms of Metals with Hydrogen Sulfide and Thiols in Model Wine. Part 2: Iron- and Copper-Catalyzed Oxidation. *J. Agric. Food. Chem.* **2016**, 64, 4105-4113. DOI: 10.1021/acs.jafc.6b00642.
- (28) (a) Perera, R.; Sono, M.; Sigman, J. A.; Pfister, T. D.; Lu, Y.; Dawson, J. H. Neutral thiol as a proximal ligand to ferrous heme iron: Implications for heme proteins that lose cysteine thiolate ligation on reduction. *Proc. Natl. Acad. Sci.* **2003**, *100*, 3641-3646. DOI: 10.1073/pnas.0737142100. (b)

- Sono, M.; Sun, S.; Modi, A.; Hargrove, M. S.; Molitor, B.; Frankenberg-Dinkel, N.; Dawson, J. H. Spectroscopic evidence supporting neutral thiol ligation to ferrous heme iron. *J. Biol. Inorg. Chem.* **2018**, 23, 1085-1092. DOI: 10.1007/s00775-018-1611-3.
- (29) (a) Buckingham, D.; Gorges, R.; Henry, J. The reaction of pyridine with iron(II) acetylacetonate in benzene solutions. *Aust. J. Chem.* **1967**, *20*, 497-502. DOI: 10.1071/CH9670497. (b) Laugier, J.; Mathieu, J. P. Structure of bisacetylacetonatoiron(II) dihydrate. *Acta Crystallogr., Sect. B: Struct. Crystallogr. Cryst. Chem.* **1975**, *B31*, 631. DOI: 10.1107/S0567740875003470. (c) Xue, Z.; Daran, J.-C.; Champouret, Y.; Poli, R. Ligand Adducts of Bis(acetylacetonato)iron(II): A <sup>1</sup>H NMR Study. *Inorg. Chem.* **2011**, *50*, 11543-11551. DOI: 10.1021/ic201486v.
- (30) Dang, H.-S.; R. J. Elsegood, M.; Kim, K.-M.; P. Roberts, B. Radicalchain reductive alkylation of electron-rich alkenes mediated by silanes in the presence of thiols as polarity-reversal catalysts. *J. Chem. Soc., Perkin Trans.* 1 1999, 2061-2068. DOI: 10.1039/A903961I.
- (31) (a) Devlin, J. P.; Hargrave, K. D. The design and synthesis of immune regulatory agents: Targets and approaches. *Tetrahedron* **1989**, *45*, 4327-4369. DOI: 10.1016/S0040-4020(01)89072-4. (b) Imming, P. Synthesis of the First Penicillin Derivatives with Medium-Sized Lactam Ring and of Related Thiazolidines. *Arch. Pharm.* **1995**, *328*, 207-215. DOI: 10.1002/ardp.19953280302. (c) Tanabe, Y.; Yamamoto, H.; Murakami, M.; Yanagi, K.; Kubota, Y.; Okumura, H.; Sanemitsu, Y.; Suzukamo, G. Synthetic study of the highly potent and selective anti-platelet activating factor thiazolidin-4-one agents and related compounds. *J. Chem. Soc., Perkin*

- Trans. 1 1995, 935-947. DOI: 10.1039/P19950000935. (d) Malešič, M.; Krbavčíč, A.; Golobič, A.; Golič, L.; Stanovnik, B. The synthesis and transformations of some 3-thiocarbamoylthiazolidines. *J. Heterocycl. Chem.* 1997, 34, 43-48. DOI: 10.1002/jhet.5570340108.
- (32) (a) Magnus, P.; Waring, M. J.; Scott, D. A. Conjugate reduction of  $\alpha$ , $\beta$ -unsaturated ketones using an Mn<sup>III</sup> catalyst, phenylsilane and isopropyl alcohol. *Tetrahedron Lett.* **2000**, *41*, 9731-9733. DOI: 10.1016/S0040-4039(00)01728-7. (b) Magnus, P.; Payne, A. H.; Waring, M. J.; Scott, D. A.; Lynch, V. Conversion of  $\alpha$ , $\beta$ -unsaturated ketones into  $\alpha$ -hydroxy ketones using an Mn<sup>III</sup> catalyst, phenylsilane and dioxygen: acceleration of conjugate hydride reduction by dioxygen. *Tetrahedron Lett.* **2000**, *41*, 9725-9730. DOI: 10.1016/S0040-4039(00)01727-5.
- (33) Lo, J. C.; Gui, J.; Yabe, Y.; Pan, C.-M.; Baran, P. S. Functionalized olefin cross-coupling to construct carbon–carbon bonds. *Nature* **2014**, *516*, 343-348. DOI: 10.1038/nature14006.
- (34) (a) Gui, J.; Pan, C.-M.; Jin, Y.; Qin, T.; Lo, J. C.; Lee, B. J.; Spergel, S. H.; Mertzman, M. E.; Pitts, W. J.; La Cruz, T. E.; Schmidt, M. A.; Darvatkar, N.; Natarajan, S. R.; Baran, P. S. Practical olefin hydroamination with nitroarenes. *Science* **2015**, 348, 886-891. DOI: doi:10.1126/science.aab0245. (b) Elfert, J.; Bhunia, A.; Daniliuc, C. G.; Studer, A. Intramolecular Radical Oxygen-Transfer Reactions Using Nitroarenes. *ACS Catal.* **2023**, 13, 6704-6709. DOI: 10.1021/acscatal.3c00958.

## **Graphical Abstract**

